Kalman Filtering for Relative Spacecraft Attitude and Position Estimation

5 authors, including:

John Crassidis
University at Buffalo, The State University of New York
260 PUBLICATIONS **10,194** CITATIONS

SEE PROFILE

Yang Cheng
XAnalytix Systems LLC
23 PUBLICATIONS **3,012** CITATIONS

SEE PROFILE

John Junkins
Texas A&M University
478 PUBLICATIONS **14,693** CITATIONS

SEE PROFILE

Kalman Filtering for Relative Spacecraft
Attitude and Position Estimation

Son-Goo Kim,[*]   John L. Crassidis,[†]   Yang Cheng,[‡]   Adam M. Fosbury[§]

University at Buffalo, State University of New York, Amherst, NY 14260-4400

John L. Junkins[¶]

Texas A&M University, College Station, TX 77843-3141

In this paper a novel approach is developed for relative navigation and attitude estimation of spacecraft flying in formation. The approach uses information from an optical sensor, which employs relatively simple electronic circuits with modest digital signal processing requirements, to provide multiple line-of-sight vectors from spacecraft to another. The sensor mechanism is well suited for both near-Earth and deep space applications since it is fully independent of any external systems. The line-of-sight measurements are coupled with gyro measurements and dynamical models in an extended Kalman filter to determine relative attitude, position and gyro biases. The quaternion is used to describe the relative kinematics and general relative orbital equations are used to describe the positional dynamics. Simulation results indicate that the combined sensor/estimator approach provides accurate relative position and attitude estimates.

I.   Introduction

Spacecraft formation flying is an important technology, but not a new concept anymore.[1,2] Since the early days of the space program several formation flying applications, such as rendezvous and docking maneuvers, have been accomplished in practice. Modern day spacecraft formation flying applications include long baseline interferometry, stereographic imaging, synthetic apertures, and distinguishing spatial from temporal magnetospheric variations. Many missions, in particular interferometry missions, rely on precise relative position and attitude knowledge in order to maintain mission requirements. To date most research studies into determining relative positions and attitudes between vehicles have involved using the Global Positioning System (GPS),[3] which restricts the spacecraft formation to near-Earth applications. An application of GPS-like technology to a deep space mission has been proposed,[4] but this requires extensive hardware development and is subject to the generic GPS performance-limiting effects, including multipath, geometric dilution of precision, integer ambiguity resolution and cycle slip. The main objective of this paper is to provide a novel, reliable and autonomous relative navigation and attitude determination system, employing relatively simple electronic circuits with modest digital signal processing requirements, and being fully independent of any external systems.

The sensor measurements using in this paper are based on a vision-based navigation (VISNAV) system which comprises an optical sensor of a new kind combined with specific light sources (beacons) in order to achieve a selective or "intelligent" vision. The sensor is made up of a Position Sensing Diode (PSD) placed in the focal plane of a wide angle lens. When the rectangular silicon area of the PSD is illuminated

[*]Graduate Student, Department of Mechanical & Aerospace Engineering. Email: sk242@eng.buffalo.edu. Student Member AIAA.

[†]Associate Professor, Department of Mechanical & Aerospace Engineering. Email: johnc@eng.buffalo.edu. Associate Fellow AIAA.

[‡]Postdoctoral Research Fellow, Department of Mechanical & Aerospace Engineering. Email: cheng3@eng.buffalo.edu. Member AIAA.

[§]Graduate Student, Department of Mechanical & Aerospace Engineering. Email: fosbury@eng.buffalo.edu. Student Member AIAA.

[¶]George J. Eppright Chair Professor, Department of Aerospace Engineering. Email: junkins@tamu.edu. Fellow AIAA.

by energy from a beacon focused by the lens, it generates electrical currents in four directions that can be processed with appropriate electronic equipment to estimate the energy centroid of the image. While the individual currents depend on the intensity of the light, their imbalances are weakly dependent on the intensity and are almost linearly proportional to the location of the centroid of the energy incident on the PSD. The idea behind the concept of intelligent vision is that the PSD can be used to see only specific light sources, accomplished by frequency domain modulation of the target lights and some relatively simple analog signal processing (demodulation). The light is produced by LEDs (beacons) modulated at an arbitrary known frequency while the currents generated are driven through an active filter set on the same frequency. Calculating the current imbalances then yields two analog signals directly related to the coordinates locating the centroid of that beacon's energy distribution on the PSD, in a quasi-linear fashion, and therefore to the incident direction of this light on the wide-angle lens (which gives a line-of-sight vector). Benefits of this configuration include: 1) very small sensor size, 2) very wide sensor field-of-view (FOV), 3) no complex/time consuming charge-coupling-device signal processing or pattern recognition required, 4) excellent rejection of ambient light interference under a wide variety of operating conditions, and 5) relatively simple electronic circuits with modest digital signal processing micro-computer requirements. These benefits clearly make the VISNAV system a viable sensor for relative navigation and attitude determination of spacecraft in formation.[5] A more detailed description of the VISNAV system can be found in Ref. 6.

This paper presents an extended Kalman filter (EKF) formulation to estimate the relative attitude and position of two spacecraft using the VISNAV sensor approach coupled with gyro measurements from each spacecraft. The attitude kinematics are based on the quaternion. Three different formulations are presented. The first estimates the relative attitude and individual gyro biases for the chief and deputy spacecraft. The second estimates the relative attitude, and the relative rate bias and the deputy gyro bias. The third estimates the relative attitude, and the relative rate bias and the chief gyro bias. The analysis of relative position motion of spacecraft also have been a key issue for planning formation flying and orbital rendezvous missions. In the early 1960's, Clohessy and Wiltshire (CW) formulated a set of simple linear relative equations of motion, derived by assuming small deviations from a circular reference orbit with no perturbations.[7,8] Others have generalized the CW equations for eccentric reference orbits,[9] and to include perturbations and higher-order nonlinear effects.[10] Another interesting approach formulates the relative motion in spherical coordinates in order to derive second-order expressions.[11] In this paper the nonlinear relative equations of motions are used in cartesian components with no external disturbances.[12] Other formulations that include disturbances can be easily derived if necessary.

The organization of this paper proceeds as follows. First, an overview of the relative coordinates systems and positional equations of motion is given. Then, the basic equations for the VISNAV system and gyro models are shown. Next, a review of the quaternion kinematics is provided, followed by a derivation of the relative attitude motion equations. Next, an EKF is derived for attitude estimation only, which assumes that the relative positions are known. Then, the relative position equations are appended to the state vector in order to perform full attitude and position estimation. Finally, simulation results are presented.

II.   Overview

In this section an overview of the frames used to describe the relative position and attitude equations of motion is shown. The measurements equations for the VISNAV sensor, which provides line-of-sight (LOS) vectors from one spacecraft to another, are then derived. Also, standard gyro measurement equations are shown, which will be used for relative attitude estimation.

A.   Relative Orbital Motion Equations

The spacecraft about which all other spacecraft are orbiting is referred to as the chief. The remaining spacecraft are referred to as the deputies. The relative orbit position vector, $\boldsymbol{\rho}$, is expressed in components by $\boldsymbol{\rho} = [x \ y \ z]^T$. A complete derivation of the relative equations of motion for eccentric orbits can be found in Ref. 12. If the relative orbit coordinates are small compared to the chief orbit radius, then the equations
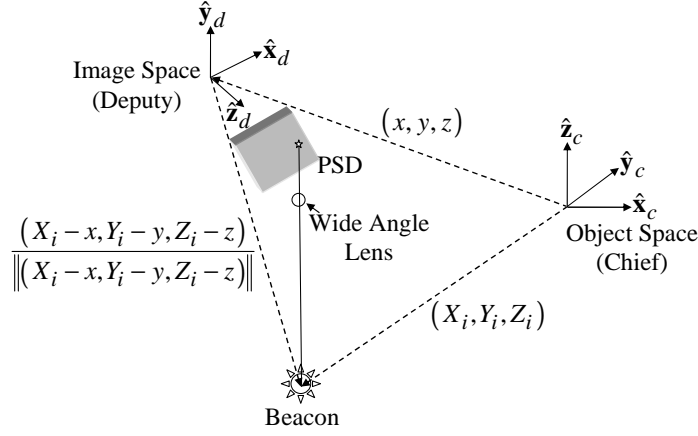
Figure 1. General Type of Spacecraft Formation with Relative Motion

of motion are given by

$$\ddot{x} - x\,\dot{\theta}^2\left(1 + 2\frac{r_c}{p}\right) - 2\,\dot{\theta}\left(\dot{y} - y\frac{\dot{r}_c}{r_c}\right) = w_x \tag{1a}$$

$$\ddot{y} + 2\,\dot{\theta}\left(\dot{x} - x\frac{\dot{r}_c}{r_c}\right) - y\,\dot{\theta}^2\left(1 - \frac{r_c}{p}\right) = w_y \tag{1b}$$

$$\ddot{z} + z\,\dot{\theta}^2\frac{r_c}{p} = w_z \tag{1c}$$

where p is semilatus rectum of the chief, r_c is the chief orbit radius and $\dot{\theta}$ is true anomaly rate of the chief. Also, w_x, w_y and w_z are acceleration disturbances which are modelled as zero-mean Gaussian white-noise processes. The true anomaly acceleration and chief orbit-radius acceleration are given by

$$\ddot{\theta} = -2\frac{\dot{r}_c}{r_c}\dot{\theta} \tag{2a}$$

$$\ddot{r}_c = r_c\,\dot{\theta}^2\left(1 - \frac{r_c}{p}\right) \tag{2b}$$

If the chief satellite orbit is assumed to be circular so that $\dot{r}_c = 0$ and $p = r_c$, then the relative equations of motion reduce to the simple form known as the CW equations (with disturbances added here):

$$\ddot{x} - 2\,n\,\dot{y} - 3\,n^2 x = w_x \tag{3a}$$

$$\ddot{y} + 2\,n\,\dot{x} = w_y \tag{3b}$$

$$\ddot{z} + n^2 z = w_z \tag{3c}$$

where $n = \dot{\theta}$ is the mean motion.

B. Vision Based Navigation System and Gyro Model

Photogrammetry is the technique of measuring objects (2D or 3D) from photographic images or LOS measurements. Photogrammetry can generally be divided into two categories: far range photogrammetry with camera distance settings to infinity (commonly used in star cameras[13]), and close range photogrammetry with camera distance settings to finite values. In general close range photogrammetry can be used to determine both the position and attitude of an object, while far range photogrammetry can only be used to determine attitude. The VISNAV system comprises an optical sensor of a new kind combined with specific light sources (beacons), which can be used for close range photogrammetry-type applications. The relationship between the position/attitude and the observations used in photogrammetry involves a set of colinearity

Figure 2. Vision Based Navigation System

equations, which are reviewed in this section. Figure 2 shows a schematic of the typical quantities involved in basic photogrammetry from LOS measurements, derived from light beacons in this case. It is assumed that the location of the sensor focal plane is known within the deputy spacecraft coordinate system, which is usually obtained through calibration. Also, without loss in generality, we assume that the chief spacecraft frame coincides with the frame describe in Figure 1. If we choose the z-axis of the sensor coordinate system to be directed outward along the boresight, then given object space and image space coordinate frames (see Figure 2), the ideal object to image space projective transformation (noiseless) can be written as follows:[14]

$$\chi_i = -f\frac{A_{11}(X_i - x) + A_{12}(Y_i - y) + A_{13}(Z_i - z)}{A_{31}(X_i - x) + A_{32}(Y_i - y) + A_{33}(Z_i - z)}, \quad i = 1, 2, \ldots, N \tag{4a}$$

$$\gamma_i = -f\frac{A_{21}(X_i - x) + A_{22}(Y_i - y) + A_{23}(Z_i - z)}{A_{31}(X_i - x) + A_{32}(Y_i - y) + A_{33}(Z_i - z)}, \quad i = 1, 2, \ldots, N \tag{4b}$$

where N is the total number of observations, (χ_i, γ_i) are the image space observations for the ith LOS, (X_i, Y_i, Z_i) are the known object space locations of the ith beacon, (x, y, z) are the unknown object space location of the sensor modelled by Eq. (1), f is the known focal length, and A_{jk} are the unknown coefficients of the attitude matrix, A, associated to the orientation from the object plane (chief) to the image plane (deputy). The goal of the *inverse problem* is given observations (χ_i, γ_i) and object space locations (X_i, Y_i, Z_i), for $i = 1, 2, \ldots, N$, determine the attitude (A) and position (x, y, z).

The observation can be reconstructed in unit vector form as

$$\mathbf{b}_i = A\mathbf{r}_i, \quad i = 1, 2, \ldots, N \tag{5}$$

where

$$\mathbf{b}_i \equiv \frac{1}{\sqrt{f^2 + \chi_i^2 + \gamma_i^2}} \begin{bmatrix} -\chi_i \\ -\gamma_i \\ f \end{bmatrix} \tag{6a}$$

$$\mathbf{r}_i \equiv \frac{1}{\sqrt{(X_i - x)^2 + (Y_i - y)^2 + (Z_i - z)^2}} \begin{bmatrix} X_i - x \\ Y_i - y \\ Z_i - z \end{bmatrix} \tag{6b}$$

When measurement noise is present, Shuster[15] has shown that nearly all the probability of the errors is concentrated on a very small area about the direction of $A\mathbf{r}_i$, so the sphere containing that point can be approximated by a tangent plane, characterized by

$$\tilde{\mathbf{b}}_i = A\mathbf{r}_i + \boldsymbol{v}_i, \quad \boldsymbol{v}_i^T A\mathbf{r}_i = 0 \tag{7}$$

American Institute of Aeronautics and Astronautics

where $\tilde{\mathbf{b}}_i$ denotes the ith measurement, and the sensor error $\boldsymbol{v}_i$ is approximately Gaussian which satisfies

$$E\{\boldsymbol{v}_i\} = \mathbf{0} \tag{8a}$$

$$E\{\boldsymbol{v}_i\boldsymbol{v}_i^T\} = \sigma_i^2\left[I_{3\times3} - (A\mathbf{r}_i)(A\mathbf{r}_i)^T\right] \tag{8b}$$

and $E\{\ \}$ denotes expectation and $I_{3\times3}$ denotes a 3×3 identity matrix. Equation (8b) makes the small FOV assumption of Ref. [15]; however, for a large FOV lens with significant radial distortion, this covariance model should be modified appropriately.[16] The advantage of using the model in Eq. (8) is that the measurement covariance in the EKF formulation can effectively be replaced by a nonsingular matrix given by $\sigma_i^2 I_{3\times3}$ (see Ref. 17 for more details). Hence, the measurement covariance matrix used in the EKF from all available LOS vectors is given by

$$R_k = \text{diag}\begin{bmatrix}\sigma_1^2 & \sigma_2^2 & \dots & \sigma_N^2\end{bmatrix} \odot I_{3\times3} \tag{9}$$

where "diag" denotes a diagonal matrix and $\odot$ denotes the Kronecker tensor product.

A common sensor that measures the angular rate is a rate-integrating gyro. For this sensor, a widely used model is given by[18]

$$\tilde{\boldsymbol{\omega}} = \boldsymbol{\omega} + \boldsymbol{\beta} + \boldsymbol{\eta}_v \tag{10a}$$

$$\dot{\boldsymbol{\beta}} = \boldsymbol{\eta}_u \tag{10b}$$

where $\boldsymbol{\omega}$ is the continuous-time true angular rate, $\tilde{\boldsymbol{\omega}}$ is the measured rate, $\boldsymbol{\beta}$ is the drift, and $\boldsymbol{\eta}_v$ and $\boldsymbol{\eta}_u$ are independent zero-mean Gaussian white-noise processes with

$$E\{\boldsymbol{\eta}_v(t)\boldsymbol{\eta}_v^T(\tau)\} = I_{3\times3}\sigma_v^2\delta(t-\tau) \tag{11a}$$

$$E\{\boldsymbol{\eta}_u(t)\boldsymbol{\eta}_u^T(\tau)\} = I_{3\times3}\sigma_u^2\delta(t-\tau) \tag{11b}$$

where $\delta(t-\tau)$ is the Dirac delta function. In this paper we use $(\boldsymbol{\eta}_{cv}, \boldsymbol{\eta}_{cu})$ and $(\boldsymbol{\eta}_{dv}, \boldsymbol{\eta}_{du})$ to denote the parameters of chief and deputy gyros, respectively. It is important to note that gyros measure with respect to an inertial frame, not with respect to the frames used to the describe the chief and deputy spacecraft shown in this section.

III.   Relative Attitude Kinematics

In this section a brief review of the attitude kinematics equation of motion using the quaternion is shown, as well as some useful identities. Then, the relative attitude kinematics between two spacecraft are shown, followed by a closed-form solution of the relative state transition matrix.

A.   Quaternion Kinematics

In this section a brief review of the quaternion kinematics is shown. More details are given in Ref. 19. The quaternion is defined by $\mathbf{q} \equiv \begin{bmatrix}\boldsymbol{\varrho}^T & q_4\end{bmatrix}^T$, with $\boldsymbol{\varrho} \equiv \begin{bmatrix}q_1 & q_2 & q_3\end{bmatrix}^T = \hat{\mathbf{e}}\sin(\vartheta/2)$ and $q_4 = \cos(\vartheta/2)$, where $\hat{\mathbf{e}}$ is the axis of rotation and ϑ is the angle of rotation.[19] Since a four-dimensional vector is used to describe three dimensions, the quaternion components cannot be independent of each other. The quaternion satisfies a single constraint given by $\|\mathbf{q}\| = 1$. The attitude matrix is related to the quaternion by

$$A(\mathbf{q}) = \Xi^T(\mathbf{q})\Psi(\mathbf{q}) \tag{12}$$

with

$$\Xi(\mathbf{q}) \equiv \begin{bmatrix}q_4 I_{3\times3} + [\boldsymbol{\varrho}\times] \\ -\boldsymbol{\varrho}^T\end{bmatrix} \tag{13a}$$

$$\Psi(\mathbf{q}) \equiv \begin{bmatrix}q_4 I_{3\times3} - [\boldsymbol{\varrho}\times] \\ -\boldsymbol{\varrho}^T\end{bmatrix} \tag{13b}$$

where $[\boldsymbol{\varrho}\times]$ is a cross product matrix since $\mathbf{a} \times \mathbf{b} = [\mathbf{a}\times]\mathbf{b}$, with

$$[\mathbf{a}\times] \equiv \begin{bmatrix} 0 & -a_3 & a_2 \\ a_3 & 0 & -a_1 \\ -a_2 & a_1 & 0 \end{bmatrix} \tag{14}$$

Successive rotations can be accomplished using quaternion multiplication. Here we adopt the convention of Ref. [20] who multiply the quaternions in the same order as the attitude matrix multiplication: $A(\mathbf{q}')A(\mathbf{q}) = A(\mathbf{q}' \otimes \mathbf{q})$. The composition of the quaternions is bilinear, with

$$\mathbf{q}' \otimes \mathbf{q} = \left[\Psi(\mathbf{q}') \vdots \mathbf{q}' \right] \mathbf{q} = \left[\Xi(\mathbf{q}) \vdots \mathbf{q} \right] \mathbf{q}' \tag{15}$$

Also, the inverse quaternion is given by $\mathbf{q}^{-1} = \begin{bmatrix} -\boldsymbol{\varrho}^T & q_4 \end{bmatrix}^T$. Note that $\mathbf{q} \otimes \mathbf{q}^{-1} = [0\ 0\ 0\ 1]^T$, which is the identity quaternion.

The quaternion kinematics equation is given by

$$\dot{\mathbf{q}} = \frac{1}{2}\Xi(\mathbf{q})\boldsymbol{\omega} = \frac{1}{2}\Omega(\boldsymbol{\omega})\mathbf{q} \tag{16}$$

where

$$\Omega(\boldsymbol{\omega}) \equiv \begin{bmatrix} -[\boldsymbol{\omega}\times] & \boldsymbol{\omega} \\ -\boldsymbol{\omega}^T & 0 \end{bmatrix} \tag{17}$$

Some useful identities are given by

$$\Xi^T(\mathbf{q})\Xi(\mathbf{q}) = \Psi^T(\mathbf{q})\Psi(\mathbf{q}) = I_{3\times3} \tag{18a}$$

$$\Xi(\mathbf{q})\Xi^T(\mathbf{q}) = \Psi(\mathbf{q})\Psi^T(\mathbf{q}) = I_{4\times4} - \mathbf{q}\mathbf{q}^T \tag{18b}$$

$$\Xi^T(\mathbf{q})\mathbf{q} = \Psi^T(\mathbf{q})\mathbf{q} = \mathbf{0}_{3\times1} \tag{18c}$$

$$\begin{bmatrix} \boldsymbol{\omega} \\ 0 \end{bmatrix} \otimes \mathbf{q} = \Omega(\boldsymbol{\omega})\mathbf{q} \tag{18d}$$

$$\mathbf{q} \otimes \begin{bmatrix} \boldsymbol{\omega} \\ 0 \end{bmatrix} = \Gamma(\boldsymbol{\omega})\mathbf{q} \tag{18e}$$

$$\Psi(\mathbf{q})\boldsymbol{\omega} = \Gamma(\boldsymbol{\omega})\mathbf{q} \tag{18f}$$

where

$$\Gamma(\boldsymbol{\omega}) \equiv \begin{bmatrix} [\boldsymbol{\omega}\times] & \boldsymbol{\omega} \\ -\boldsymbol{\omega}^T & 0 \end{bmatrix} \tag{19}$$

It is assumed in Eqs. (18a) and (18b) that $||\mathbf{q}|| = 1$. Also, $\Omega(\mathbf{a})$ and $\Gamma(\mathbf{b})$ commute for any $\mathbf{a}$ and $\mathbf{b}$, so that $\Omega(\mathbf{a})\Gamma(\mathbf{b}) = \Gamma(\mathbf{b})\Omega(\mathbf{a})$.

B.   Relative Kinematics

In this section a review of the relative quaternion kinematics is shown. Also, a solution of the associated state transition matrix is derived. The relative attitude, denoted by the quaternion $\mathbf{q}$, which is used to map vectors in the chief frame to vectors in the deputy frame is expressed by

$$\mathbf{q} = \mathbf{q}_d \otimes \mathbf{q}_c^{-1} \tag{20}$$

where $\mathbf{q}_d$ and $\mathbf{q}_c$ are the attitudes of the chief (leader) and deputy (follower) spacecraft, respectively. Equation (20) is similar to the error quaternion used in Kalman filtering. Following Ref. 20, the relative quaternion kinematics can be shown to be given by

$$\dot{\mathbf{q}} = -\begin{bmatrix} [\boldsymbol{\omega}_c\times]\boldsymbol{\varrho} \\ 0 \end{bmatrix} + \frac{1}{2}\begin{bmatrix} (\boldsymbol{\omega}_d - \boldsymbol{\omega}_c) \\ 0 \end{bmatrix} \otimes \mathbf{q} \tag{21}$$

American Institute of Aeronautics and Astronautics

where $\boldsymbol{\omega}_c$ and $\boldsymbol{\omega}_d$ are the angular velocities of the chief and deputy, respectively. Equation (21) is equivalent to the kinematics shown in Ref. 21:

$$\dot{\mathbf{q}} = \frac{1}{2}\Xi(\mathbf{q})\boldsymbol{\omega}_{dc} \tag{22}$$

where $\boldsymbol{\omega}_{dc}$ is the relative angular velocity defined by

$$\boldsymbol{\omega}_{dc} \equiv \boldsymbol{\omega}_d - A(\mathbf{q})\boldsymbol{\omega}_c \tag{23}$$

Equation (22) can be simplified by substituting Eq. (12) into Eq. (23) and using the identities in Eqs. (16), (18b), (18c) and (18f), which yields

$$\dot{\mathbf{q}} = \frac{1}{2}\Theta(\boldsymbol{\omega}_d,\, \boldsymbol{\omega}_c)\mathbf{q} \tag{24}$$

where $\Theta(\boldsymbol{\omega}_d,\, \boldsymbol{\omega}_c) \equiv \Omega(\boldsymbol{\omega}_d) - \Gamma(\boldsymbol{\omega}_c)$.

We now show a closed-form solution for the state transition matrix of $\frac{1}{2}\Theta(\boldsymbol{\omega}_d,\, \boldsymbol{\omega}_c)$. As an aside, note that the eigenvalues of this matrix are given by $\pm(||\boldsymbol{\omega}_d|| + ||\boldsymbol{\omega}_c||)j$ and $\pm(||\boldsymbol{\omega}_d|| - ||\boldsymbol{\omega}_c||)j$. Since the matrices $\Omega(\boldsymbol{\omega}_d)$ and $\Gamma(\boldsymbol{\omega}_c)$ commute, we can write

$$\exp\left[\frac{1}{2}\Theta(\boldsymbol{\omega}_d,\, \boldsymbol{\omega}_c)t\right] = \exp\left[\frac{1}{2}\Omega(\boldsymbol{\omega}_d)t\right]\exp\left[-\frac{1}{2}\Gamma(\boldsymbol{\omega}_c)t\right] \tag{25}$$

The closed-form solution for the matrix exponential of $\frac{1}{2}\Omega(\boldsymbol{\omega}_d)t$ is well documented (see Ref. 22). Applying a similar derivation to the matrix $-\frac{1}{2}\Gamma(\boldsymbol{\omega}_c)t$ gives

$$\exp\left[-\frac{1}{2}\Gamma(\boldsymbol{\omega}_c)t\right] = I_{4\times4}\cos\left(\frac{1}{2}||\boldsymbol{\omega}_c||t\right) - \Gamma(\boldsymbol{\omega}_c)\frac{\sin\left(\frac{1}{2}||\boldsymbol{\omega}_c||t\right)}{||\boldsymbol{\omega}_c||} \tag{26}$$

Hence, the discrete-time propagation of the relative quaternion is given by

$$\mathbf{q}_{k+1} = \bar{\Omega}(\boldsymbol{\omega}_{d_k})\bar{\Gamma}(\boldsymbol{\omega}_{c_k})\mathbf{q}_k \tag{27}$$

with

$$\bar{\Omega}(\boldsymbol{\omega}_{d_k}) \equiv \begin{bmatrix} \cos\left(\frac{1}{2}||\boldsymbol{\omega}_{d_k}||\,\Delta t\right)I_{3\times3} - [\boldsymbol{\psi}_k\times] & \boldsymbol{\psi}_k \\[2em] -\boldsymbol{\psi}_k^T & \cos\left(\frac{1}{2}||\boldsymbol{\omega}_{d_k}||\,\Delta t\right) \end{bmatrix} \tag{28a}$$

$$\bar{\Gamma}(\boldsymbol{\omega}_{c_k}) \equiv \begin{bmatrix} \cos\left(\frac{1}{2}||\boldsymbol{\omega}_{c_k}||\,\Delta t\right)I_{3\times3} - [\boldsymbol{\zeta}_k\times] & -\boldsymbol{\zeta}_k \\[2em] \boldsymbol{\zeta}_k^T & \cos\left(\frac{1}{2}||\boldsymbol{\omega}_{c_k}||\,\Delta t\right) \end{bmatrix} \tag{28b}$$

where

$$\boldsymbol{\psi}_k \equiv \frac{\sin\left(\frac{1}{2}||\boldsymbol{\omega}_{d_k}||\,\Delta t\right)\boldsymbol{\omega}_{d_k}}{||\boldsymbol{\omega}_{d_k}||} \tag{29a}$$

$$\boldsymbol{\zeta}_k \equiv \frac{\sin\left(\frac{1}{2}||\boldsymbol{\omega}_{c_k}||\,\Delta t\right)\boldsymbol{\omega}_{c_k}}{||\boldsymbol{\omega}_{c_k}||} \tag{29b}$$

and Δt is the sampling interval. Note that the matrices $\bar{\Omega}(\boldsymbol{\omega}_{d_k})$ and $\bar{\Gamma}(\boldsymbol{\omega}_{c_k})$ also commute.

IV. Relative Attitude Estimation

In this section the necessary equations for relative attitude estimation between two spacecraft are derived. The estimator used for this relative estimation is based on the EKF. A review of the EKF equations can be found in Ref. 23. In this section it is assumed that the relative position is known, and only the attitude and gyro biases will be estimated. In the next section, relative position estimation will be implemented as well. Three attitude estimation formulations are presented here. The first estimates the relative attitude and individual gyro biases for the chief and deputy spacecraft. The second estimates the relative attitude, and the relative rate bias and the deputy gyro bias. The third estimates the relative attitude, and the relative rate bias and the chief gyro bias.

A. Chief and Deputy Gyro Bias Case

In this section a formulation to estimate the relative attitude, as well as the chief and deputy gyro biases is derived. The truth equations are given by

$$\dot{\mathbf{q}} = \frac{1}{2}\Xi(\mathbf{q})\boldsymbol{\omega}_{dc} \tag{30a}$$

$$\boldsymbol{\omega}_{dc} = \boldsymbol{\omega}_d - A(\mathbf{q})\boldsymbol{\omega}_c \tag{30b}$$

$$\dot{\boldsymbol{\beta}}_c = \boldsymbol{\eta}_{cu} \tag{30c}$$

$$\dot{\boldsymbol{\beta}}_d = \boldsymbol{\eta}_{du} \tag{30d}$$

$$\boldsymbol{\omega}_c = \tilde{\boldsymbol{\omega}}_c - \boldsymbol{\beta}_c - \boldsymbol{\eta}_{cv} \tag{30e}$$

$$\boldsymbol{\omega}_d = \tilde{\boldsymbol{\omega}}_d - \boldsymbol{\beta}_d - \boldsymbol{\eta}_{dv} \tag{30f}$$

The estimates are given by

$$\dot{\hat{\mathbf{q}}} = \frac{1}{2}\Xi(\hat{\mathbf{q}})\hat{\boldsymbol{\omega}}_{dc} \tag{31a}$$

$$\hat{\boldsymbol{\omega}}_{dc} = \hat{\boldsymbol{\omega}}_d - A(\hat{\mathbf{q}})\hat{\boldsymbol{\omega}}_c \tag{31b}$$

$$\dot{\hat{\boldsymbol{\beta}}}_c = \mathbf{0} \tag{31c}$$

$$\dot{\hat{\boldsymbol{\beta}}}_d = \mathbf{0} \tag{31d}$$

$$\hat{\boldsymbol{\omega}}_c = \tilde{\boldsymbol{\omega}}_c - \hat{\boldsymbol{\beta}}_c \tag{31e}$$

$$\hat{\boldsymbol{\omega}}_d = \tilde{\boldsymbol{\omega}}_d - \hat{\boldsymbol{\beta}}_d \tag{31f}$$

Note that the quaternion kinematics involves the attitude matrix. To provide a set of linearized equations used in the covariance propagation in the EKF, we employ the linearization approach shown in Ref. 20. The error quaternion and its derivative are given by

$$\boldsymbol{\delta q} = \mathbf{q} \otimes \hat{\mathbf{q}}^{-1} \tag{32a}$$

$$\boldsymbol{\delta\dot{q}} = \dot{\mathbf{q}} \otimes \hat{\mathbf{q}}^{-1} + \mathbf{q} \otimes \dot{\hat{\mathbf{q}}}^{-1} \tag{32b}$$

The derivative of $\hat{\mathbf{q}}^{-1}$ can be derived by taking the derivative of $\hat{\mathbf{q}} \otimes \hat{\mathbf{q}}^{-1} = [0\ 0\ 0\ 1]^T$, which leads to

$$\dot{\hat{\mathbf{q}}}^{-1} = -\frac{1}{2}\hat{\mathbf{q}}^{-1} \otimes \begin{bmatrix} \hat{\boldsymbol{\omega}}_{dc} \\ 0 \end{bmatrix} \tag{33}$$

Substituting Eqs. (30a) and (33) into Eq. (32b) leads to

$$\boldsymbol{\delta\dot{q}} = \frac{1}{2}\begin{bmatrix} \boldsymbol{\omega}_{dc} \\ 0 \end{bmatrix} \otimes \boldsymbol{\delta q} - \frac{1}{2}\boldsymbol{\delta q} \otimes \begin{bmatrix} \hat{\boldsymbol{\omega}}_{dc} \\ 0 \end{bmatrix} \tag{34}$$

Next, we define the following error variables: $\boldsymbol{\delta\omega}_d \equiv \boldsymbol{\omega}_d - \hat{\boldsymbol{\omega}}_d$ and $\boldsymbol{\delta\omega}_c \equiv \boldsymbol{\omega}_c - \hat{\boldsymbol{\omega}}_c$. Using these definitions in $\boldsymbol{\omega}_{dc}$ gives

$$\boldsymbol{\omega}_{dc} = \hat{\boldsymbol{\omega}}_d - A(\mathbf{q})\hat{\boldsymbol{\omega}}_c + \boldsymbol{\delta\omega}_d - A(\mathbf{q})\boldsymbol{\delta\omega}_c \tag{35}$$

The linearization process make the following assumptions, which are valid to within first-order:[20]

$$\delta \mathbf{q} = \begin{bmatrix} \frac{1}{2}\delta\boldsymbol{\alpha} \\ 1 \end{bmatrix} \tag{36a}$$

$$A(\mathbf{q}) = \{I_{3\times3} - [\delta\boldsymbol{\alpha}\times]\} A(\hat{\mathbf{q}}) \tag{36b}$$

where $\delta\boldsymbol{\alpha}$ is a small angle-error correction. Substituting Eq. (36b) into Eq. (35) and neglecting second-order effects leads to

$$\boldsymbol{\omega}_{dc} = \hat{\boldsymbol{\omega}}_{dc} - [A(\hat{\mathbf{q}})\hat{\boldsymbol{\omega}}_c\times]\delta\boldsymbol{\alpha} + \delta\boldsymbol{\omega}_d - A(\hat{\mathbf{q}})\delta\boldsymbol{\omega}_c \tag{37}$$

Substituting Eqs. (36a) and (37) into Eq. (34), and again neglecting second-order effects leads to

$$\delta\dot{\boldsymbol{\alpha}} = -[\hat{\boldsymbol{\omega}}_d\times]\delta\boldsymbol{\alpha} + \delta\boldsymbol{\omega}_d - A(\hat{\mathbf{q}})\delta\boldsymbol{\omega}_c \tag{38}$$

The derivative of the fourth error quaternion component is zero. Next, using $\delta\boldsymbol{\omega}_d = -(\Delta\boldsymbol{\beta}_d + \boldsymbol{\eta}_{dv})$ and $\delta\boldsymbol{\omega}_c = -(\Delta\boldsymbol{\beta}_c + \boldsymbol{\eta}_{cv})$, where $\Delta\boldsymbol{\beta}_d \equiv \boldsymbol{\beta}_d - \hat{\boldsymbol{\beta}}_d$ and $\Delta\boldsymbol{\beta}_c \equiv \boldsymbol{\beta}_c - \hat{\boldsymbol{\beta}}_c$, in Eq. (38) leads to

$$\delta\dot{\boldsymbol{\alpha}} = -[\hat{\boldsymbol{\omega}}_d\times]\delta\boldsymbol{\alpha} - \Delta\boldsymbol{\beta}_d + A(\hat{\mathbf{q}})\Delta\boldsymbol{\beta}_c + A(\hat{\mathbf{q}})\boldsymbol{\eta}_{cv} - \boldsymbol{\eta}_{dv} \tag{39}$$

The error-state dynamics are now given by

$$\Delta\dot{\mathbf{x}} = F\Delta\mathbf{x} + G\mathbf{w} \tag{40}$$

with

$$\Delta\mathbf{x} \equiv \begin{bmatrix} \delta\boldsymbol{\alpha}^T & \Delta\boldsymbol{\beta}_c^T & \Delta\boldsymbol{\beta}_d^T \end{bmatrix}^T \tag{41a}$$

$$\mathbf{w} \equiv \begin{bmatrix} \boldsymbol{\eta}_{cv}^T & \boldsymbol{\eta}_{dv}^T & \boldsymbol{\eta}_{cu}^T & \boldsymbol{\eta}_{du}^T \end{bmatrix}^T \tag{41b}$$

where

$$F = \begin{bmatrix} -[\hat{\boldsymbol{\omega}}_d\times] & A(\hat{\mathbf{q}}) & -I_{3\times3} \\ 0_{3\times3} & 0_{3\times3} & 0_{3\times3} \\ 0_{3\times3} & 0_{3\times3} & 0_{3\times3} \end{bmatrix} \tag{42a}$$

$$G = \begin{bmatrix} A(\hat{\mathbf{q}}) & -I_{3\times3} & 0_{3\times3} & 0_{3\times3} \\ 0_{3\times3} & 0_{3\times3} & I_{3\times3} & 0_{3\times3} \\ 0_{3\times3} & 0_{3\times3} & 0_{3\times3} & I_{3\times3} \end{bmatrix} \tag{42b}$$

and the spectral density matrix of the process noise $\mathbf{w}$ is given by

$$Q = \begin{bmatrix} \sigma_{cv}^2 I_{3\times3} & 0_{3\times3} & 0_{3\times3} & 0_{3\times3} \\ 0_{3\times3} & \sigma_{dv}^2 I_{3\times3} & 0_{3\times3} & 0_{3\times3} \\ 0_{3\times3} & 0_{3\times3} & \sigma_{cu}^2 I_{3\times3} & 0_{3\times3} \\ 0_{3\times3} & 0_{3\times3} & 0_{3\times3} & \sigma_{du}^2 I_{3\times3} \end{bmatrix} \tag{43}$$

The linearization of the output (measurement) process exactly follows Ref. 20, which is not shown here.

Solutions for the state transition matrix of F and discrete-time process noise covariance are intractable due to the dependence of both on the attitude matrix. A numerical solution is given by van Loan[24] for fixed-parameter systems, which includes a constant sampling interval and time invariant state and covariance matrices. First, the following 12×12 matrix is formed:

$$\mathcal{A} = \begin{bmatrix} -F & G\,Q\,G^T \\ 0 & F^T \end{bmatrix} \Delta t \tag{44}$$

Then, the matrix exponential of Eq. (44) is computed:

$$\mathcal{B} = e^{\mathcal{A}} \equiv \begin{bmatrix} \mathcal{B}_{11} & \mathcal{B}_{12} \\ 0 & \mathcal{B}_{22} \end{bmatrix} = \begin{bmatrix} \mathcal{B}_{11} & \Phi^{-1}\mathcal{Q} \\ 0 & \Phi^T \end{bmatrix} \tag{45}$$

American Institute of Aeronautics and Astronautics

Table 1. Extended Kalman Filter for Relative Attitude Estimation

Initialize	$\hat{\mathbf{q}}(t_0) = \hat{\mathbf{q}}_0, \quad \hat{\boldsymbol{\beta}}_c(t_0) = \hat{\boldsymbol{\beta}}_{c_0} \quad \hat{\boldsymbol{\beta}}_d(t_0) = \hat{\boldsymbol{\beta}}_{d_0}$ $P(t_0) = P_0$
Gain	$K_k = P_k^- H_k^T(\hat{\mathbf{q}}_k^-)[H_k(\hat{\mathbf{q}}_k^-)P_k^- H_k^T(\hat{\mathbf{q}}_k^-) + R_k]^{-1}$ $H_k(\hat{\mathbf{q}}_k^-) = \begin{bmatrix} [A(\hat{\mathbf{q}}^-)\mathbf{r}_1\times] & 0_{3\times3} & 0_{3\times3} \\ \vdots & \vdots & \vdots \\ [A(\hat{\mathbf{q}}^-)\mathbf{r}_N\times] & 0_{3\times3} & 0_{3\times3} \end{bmatrix}\Bigg|_{t_k}$
Update	$P_k^+ = [I - K_k H_k(\hat{\mathbf{q}}_k^-)]P_k^-$ $\Delta\hat{\mathbf{x}}_k^+ = K_k[\tilde{\mathbf{y}}_k - \mathbf{h}_k(\hat{\mathbf{q}}_k^-)]$ $\Delta\hat{\mathbf{x}}_k^+ \equiv \begin{bmatrix} \boldsymbol{\delta\hat{\alpha}}_k^{+T} & \Delta\hat{\boldsymbol{\beta}}_{c_k}^{+T} & \Delta\hat{\boldsymbol{\beta}}_{d_k}^{+T} \end{bmatrix}^T$ $\mathbf{h}_k(\hat{\mathbf{q}}_k^-) = \begin{bmatrix} A(\hat{\mathbf{q}}^-)\mathbf{r}_1 \\ A(\hat{\mathbf{q}}^-)\mathbf{r}_2 \\ \vdots \\ A(\hat{\mathbf{q}}^-)\mathbf{r}_N \end{bmatrix}\Bigg|_{t_k}$ $\hat{\mathbf{q}}_k^+ = \hat{\mathbf{q}}_k^- + \frac{1}{2}\Xi(\hat{\mathbf{q}}_k^-)\boldsymbol{\delta\hat{\alpha}}_k^+$ $\hat{\boldsymbol{\beta}}_{c_k}^+ = \hat{\boldsymbol{\beta}}_{c_k}^- + \Delta\hat{\boldsymbol{\beta}}_{c_k}^+$ $\hat{\boldsymbol{\beta}}_{d_k}^+ = \hat{\boldsymbol{\beta}}_{d_k}^- + \Delta\hat{\boldsymbol{\beta}}_{d_k}^+$
Propagation	$\hat{\boldsymbol{\omega}}_{c_k}^+ = \tilde{\boldsymbol{\omega}}_{c_k} - \hat{\boldsymbol{\beta}}_{c_k}^+$ $\hat{\boldsymbol{\omega}}_{d_k}^+ = \tilde{\boldsymbol{\omega}}_{d_k} - \hat{\boldsymbol{\beta}}_{d_k}^+$ $\hat{\mathbf{q}}_{k+1}^- = \bar{\Omega}(\hat{\boldsymbol{\omega}}_{d_k}^+)\bar{\Gamma}(\hat{\boldsymbol{\omega}}_{c_k}^+)\hat{\mathbf{q}}_k^+$ $P_{k+1}^- = \Phi_k P_k^+ \Phi_k^T + \mathcal{Q}_k$

where Φ is the state transition matrix of F and $\mathcal{Q}$ is the discrete-time covariance matrix. The state transition matrix and discrete-time process noise covariance are then given by

$$\Phi = \mathcal{B}_{22}^T \tag{46a}$$
$$\mathcal{Q} = \Phi\,\mathcal{B}_{12} \tag{46b}$$

If the sampling interval is "small" enough (well within Nyquist's limit), then $\mathcal{Q} = \Delta t\, G\, Q\, G^T$ is a good approximation for the solution given by Eq. (46b).

A summary of the EKF equations for relative attitude estimation is shown in Table 1, where P is the covariance matrix that consists of the covariance of the attitude errors and chief and deputy biases, and the vector $\tilde{\mathbf{y}}$ is given by $\tilde{\mathbf{y}} = [\tilde{\mathbf{b}}_1^T \ \ \tilde{\mathbf{b}}_2^T \ \ \cdots \ \ \tilde{\mathbf{b}}_N^T]^T$. Note that the propagated gyro biases are equivalent to their respected previous-time updates. A quaternion measurement, denoted by $\tilde{\mathbf{q}}$, which can be computed when at least 4 LOS vectors are available,[25] may be used instead of body vector measurements. Then $\tilde{\mathbf{y}}_k - \mathbf{h}_k(\hat{\mathbf{q}}_k^-)$ is replaced with $2\,\Xi^T(\hat{\mathbf{q}}_k^-)\tilde{\mathbf{q}}_k$. The factor of 2 is required since the angle error is used in the EKF update. Also, $H_k(\hat{\mathbf{q}}_k^-)$ is replaced with $H_k = [I_{3\times3} \ \ 0_{3\times3} \ \ 0_{3\times3}]$ and R_k is replaced with a 3×3 matrix of the attitude errors.

The EKF provides estimates for the individual biases of the chief and deputy, which in turn are used

American Institute of Aeronautics and Astronautics

to estimate for their respective angular velocities. The estimated relative angular velocity can be computed using Eq. (31b), which is typically used in a controller, such as the one presented in Ref. 21. The covariance of the estimated relative bias, defined by $\hat{\boldsymbol{\beta}}_{dc} \equiv \hat{\boldsymbol{\beta}}_d - A(\hat{\mathbf{q}})\hat{\boldsymbol{\beta}}_c$, is useful to quantify the expected error in the relative velocity estimate. Using the error definitions of the biases and attitude, $\hat{\boldsymbol{\beta}}_{dc}$ can be expressed by

$$\hat{\boldsymbol{\beta}}_{dc} = (\boldsymbol{\beta}_d - \Delta\boldsymbol{\beta}_d) - \{I_{3\times3} + [\boldsymbol{\delta\alpha}\times]\} A(\mathbf{q})(\boldsymbol{\beta}_c - \Delta\boldsymbol{\beta}_c) \tag{47}$$

Assuming unbiased estimates gives $E\left\{\hat{\boldsymbol{\beta}}_{dc}\right\} = \boldsymbol{\beta}_d - A(\mathbf{q})\boldsymbol{\beta}_c$. Next, ignoring second-order effects leads to

$$\hat{\boldsymbol{\beta}}_{dc} - E\left\{\hat{\boldsymbol{\beta}}_{dc}\right\} = [A(\mathbf{q})\boldsymbol{\beta}_c\times]\boldsymbol{\delta\alpha} + A(\mathbf{q})\Delta\boldsymbol{\beta}_c - \Delta\boldsymbol{\beta}_d \tag{48}$$

Hence, the covariance of $\hat{\boldsymbol{\beta}}_{dc}$ is given by

$$\mathrm{cov}\left\{\hat{\boldsymbol{\beta}}_{dc}\right\} = \mathcal{H} P \mathcal{H}^T \tag{49}$$

where

$$\mathcal{H} \equiv \begin{bmatrix} [A(\mathbf{q})\boldsymbol{\beta}_c\times] & A(\mathbf{q}) & -I_{3\times3} \end{bmatrix} \tag{50}$$

and P is the covariance from the EKF. Note that $\mathcal{H}$ is evaluated at the *true* values, but must be replaced with their respective estimate values for practical purposes. This leads to second-order errors when the estimates are close to their true values.

B.   Relative and Deputy Gyro Bias Case

In this section a formulation to estimate the relative attitude, as well as the relative and deputy gyro biases is derived. Estimating for the relative bias directly is useful since the EKF gives its covariance directly in this case. The linearized equations must now involve $\hat{\boldsymbol{\beta}}_d$ and $\hat{\boldsymbol{\beta}}_{dc}$. We first derive the attitude-error equation in terms of these variables. Defining $\Delta\boldsymbol{\beta}_{dc} \equiv \boldsymbol{\beta}_{dc} - \hat{\boldsymbol{\beta}}_{dc}$, and using $\hat{\boldsymbol{\beta}}_{dc} = \hat{\boldsymbol{\beta}}_d - A(\hat{\mathbf{q}})\hat{\boldsymbol{\beta}}_c$, $\boldsymbol{\beta}_c = \hat{\boldsymbol{\beta}}_c + \Delta\boldsymbol{\beta}_c$ and Eq. (36b) leads to

$$\Delta\boldsymbol{\beta}_{dc} = [(\hat{\boldsymbol{\beta}}_{dc} - \hat{\boldsymbol{\beta}}_d)\times]\boldsymbol{\delta\alpha} + \Delta\boldsymbol{\beta}_d - A(\hat{\mathbf{q}})\Delta\boldsymbol{\beta}_c \tag{51}$$

where second-order effects are ignored. Solving Eq. (51) for $A(\hat{\mathbf{q}})\Delta\boldsymbol{\beta}_c - \Delta\boldsymbol{\beta}_d$ and substituting the resultant into Eq. (39) leads to

$$\boldsymbol{\delta\dot{\alpha}} = -[(\tilde{\boldsymbol{\omega}}_d - \hat{\boldsymbol{\beta}}_{dc})\times]\boldsymbol{\delta\alpha} - \Delta\boldsymbol{\beta}_{dc} + A(\hat{\mathbf{q}})\boldsymbol{\eta}_{cv} - \boldsymbol{\eta}_{dv} \tag{52}$$

Next, we need to determine a dynamics model for $\boldsymbol{\beta}_{dc} = \boldsymbol{\beta}_d - A(\mathbf{q})\boldsymbol{\beta}_c$. Taking the time derivative of this equation and using Eqs. (30b)-(30f) in the resulting expression yields

$$\begin{aligned}
\dot{\boldsymbol{\beta}}_{dc} = &-[(\tilde{\boldsymbol{\omega}}_d - A(\mathbf{q})\tilde{\boldsymbol{\omega}}_c - \boldsymbol{\beta}_d - \boldsymbol{\eta}_{dv} + A(\mathbf{q})\boldsymbol{\eta}_{cv})\times]\boldsymbol{\beta}_{dc} \\
&+ [(\tilde{\boldsymbol{\omega}}_d - A(\mathbf{q})\tilde{\boldsymbol{\omega}}_c - \boldsymbol{\eta}_{dv} + A(\mathbf{q})\boldsymbol{\eta}_{cv})\times]\boldsymbol{\beta}_d + \boldsymbol{\eta}_{du} - A(\mathbf{q})\boldsymbol{\eta}_{cu}
\end{aligned} \tag{53}$$

The estimate equation is given by

$$\dot{\hat{\boldsymbol{\beta}}}_{dc} = -[(\tilde{\boldsymbol{\omega}}_d - A(\hat{\mathbf{q}})\tilde{\boldsymbol{\omega}}_c - \hat{\boldsymbol{\beta}}_d)\times]\hat{\boldsymbol{\beta}}_{dc} + [(\tilde{\boldsymbol{\omega}}_d - A(\hat{\mathbf{q}})\tilde{\boldsymbol{\omega}}_c)\times]\hat{\boldsymbol{\beta}}_d \tag{54}$$

The linear dynamics of $\Delta\dot{\hat{\boldsymbol{\beta}}}_{dc}$ can be derived in a similar fashion as the other linearized equations shown to this point. For brevity this derivation is omitted here. The error-state dynamics are given by

$$\Delta\dot{\mathbf{x}} = F\Delta\mathbf{x} + G\mathbf{w} \tag{55}$$

with

$$\Delta\mathbf{x} \equiv \begin{bmatrix} \boldsymbol{\delta\alpha}^T & \Delta\boldsymbol{\beta}_{dc}^T & \Delta\boldsymbol{\beta}_d^T \end{bmatrix}^T \tag{56a}$$

$$\mathbf{w} \equiv \begin{bmatrix} \boldsymbol{\eta}_{cv}^T & \boldsymbol{\eta}_{dv}^T & \boldsymbol{\eta}_{cu}^T & \boldsymbol{\eta}_{du}^T \end{bmatrix}^T \tag{56b}$$

where

$$F = \begin{bmatrix} -[(\tilde{\boldsymbol{\omega}}_d - \hat{\boldsymbol{\beta}}_{dc})\times] & -I_{3\times3} & 0_{3\times3} \\ F_{21} & F_{22} & F_{23} \\ 0_{3\times3} & 0_{3\times3} & 0_{3\times3} \end{bmatrix} \tag{57a}$$

$$F_{21} = [(\hat{\boldsymbol{\beta}}_d - \hat{\boldsymbol{\beta}}_{dc})\times][A(\hat{\mathbf{q}})\tilde{\boldsymbol{\omega}}_c\times] \tag{57b}$$

$$F_{22} = -[(\tilde{\boldsymbol{\omega}}_d - A(\hat{\mathbf{q}})\tilde{\boldsymbol{\omega}}_c - \hat{\boldsymbol{\beta}}_d)\times] \tag{57c}$$

$$F_{23} = [(\tilde{\boldsymbol{\omega}}_d - A(\hat{\mathbf{q}})\tilde{\boldsymbol{\omega}}_c - \hat{\boldsymbol{\beta}}_{dc})\times] \tag{57d}$$

$$G = \begin{bmatrix} A(\hat{\mathbf{q}}) & -I_{3\times3} & 0_{3\times3} & 0_{3\times3} \\ -[(\hat{\boldsymbol{\beta}}_d - \hat{\boldsymbol{\beta}}_{dc})\times]A(\hat{\mathbf{q}}) & [(\hat{\boldsymbol{\beta}}_d - \hat{\boldsymbol{\beta}}_{dc})\times] & -A(\hat{\mathbf{q}}) & I_{3\times3} \\ 0_{3\times3} & 0_{3\times3} & 0_{3\times3} & I_{3\times3} \end{bmatrix} \tag{57e}$$

and the spectral density matrix of the process noise $\mathbf{w}$ is given by Eq. (43). The EKF filter equations can now be employed using the state matrices in Eq. (55) in the covariance propagation as well as Eqs. (31a), (31d) and (54) for the state propagation. We note that a closed-form solution for the state propagation equation is difficult due to the appearance of the attitude matrix in Eq. (54). However, if the sampling interval is "small enough" (within Nyquist's upper limit), then a pure discrete-time propagation can be employed by holding $\hat{\mathbf{q}}$ constant throughout the interval, while using the discrete-time quaternion propagation shown in Table 1.

C.   Relative and Chief Gyro Bias Case

In this section the necessary equations to estimate the relative attitude, as well as the relative and chief gyro biases are shown. For brevity these equations are shown without derivation. The dynamic equation for the relative bias estimate is given by

$$\dot{\hat{\boldsymbol{\beta}}}_{dc} = [A(\hat{\mathbf{q}})\hat{\boldsymbol{\beta}}_c\times]\hat{\boldsymbol{\beta}}_{dc} - [A(\hat{\mathbf{q}})\hat{\boldsymbol{\beta}}_c\times](\tilde{\boldsymbol{\omega}}_d - A(\hat{\mathbf{q}})\tilde{\boldsymbol{\omega}}_c) \tag{58}$$

The error-state dynamics are given by

$$\Delta\dot{\mathbf{x}} = F\Delta\mathbf{x} + G\mathbf{w} \tag{59}$$

with

$$\Delta\mathbf{x} \equiv \begin{bmatrix} \boldsymbol{\delta\alpha}^T & \Delta\boldsymbol{\beta}_{dc}^T & \Delta\boldsymbol{\beta}_c^T \end{bmatrix}^T \tag{60a}$$

$$\mathbf{w} \equiv \begin{bmatrix} \boldsymbol{\eta}_{cv}^T & \boldsymbol{\eta}_{dv}^T & \boldsymbol{\eta}_{cu}^T & \boldsymbol{\eta}_{du}^T \end{bmatrix}^T \tag{60b}$$

where

$$F = \begin{bmatrix} -[(\tilde{\boldsymbol{\omega}}_d - \hat{\boldsymbol{\beta}}_{dc})\times] & -I_{3\times3} & 0_{3\times3} \\ F_{21} & F_{22} & F_{23} \\ 0_{3\times3} & 0_{3\times3} & 0_{3\times3} \end{bmatrix} \tag{61a}$$

$$F_{21} = [A(\hat{\mathbf{q}})\hat{\boldsymbol{\beta}}_c\times][A(\hat{\mathbf{q}})\tilde{\boldsymbol{\omega}}_c\times] + [(\tilde{\boldsymbol{\omega}}_d - A(\hat{\mathbf{q}})\tilde{\boldsymbol{\omega}}_c - \hat{\boldsymbol{\beta}}_{dc})\times][A(\hat{\mathbf{q}})\hat{\boldsymbol{\beta}}_c\times] \tag{61b}$$

$$F_{22} = [A(\hat{\mathbf{q}})\hat{\boldsymbol{\beta}}_c\times] \tag{61c}$$

$$F_{23} = [(\tilde{\boldsymbol{\omega}}_d - A(\hat{\mathbf{q}})\tilde{\boldsymbol{\omega}}_c - \hat{\boldsymbol{\beta}}_{dc})\times]A(\hat{\mathbf{q}}) \tag{61d}$$

$$G = \begin{bmatrix} A(\hat{\mathbf{q}}) & -I_{3\times3} & 0_{3\times3} & 0_{3\times3} \\ -[A(\hat{\mathbf{q}})\hat{\boldsymbol{\beta}}_c\times]A(\hat{\mathbf{q}}) & [A(\hat{\mathbf{q}})\hat{\boldsymbol{\beta}}_c\times] & -A(\hat{\mathbf{q}}) & I_{3\times3} \\ 0_{3\times3} & 0_{3\times3} & 0_{3\times3} & I_{3\times3} \end{bmatrix} \tag{61e}$$

and the spectral density matrix of the process noise $\mathbf{w}$ is again given by Eq. (43). The EKF filter equations can now be employed using the state matrices in Eq. (59) in the covariance propagation as well as Eqs. (31a), (31c) and (58) for the state propagation.

V. Relative Attitude and Position Estimation

In this section the necessary equations for both relative attitude and position estimation between two spacecraft are derived. The state vector in the attitude-only estimation formulations shown in the previous section is now appended to include position and velocity of the deputy, radius and radial rate of the chief, and the true anomaly and its rate. This appended vector is given by

$$
\mathbf{X} = \begin{bmatrix} x & y & z & \dot{x} & \dot{y} & \dot{z} & r_c & \dot{r}_c & \theta & \dot{\theta} \end{bmatrix}^T
$$
$$
\equiv \begin{bmatrix} x_1 & x_2 & x_3 & x_4 & x_5 & x_6 & x_7 & x_8 & x_9 & x_{10} \end{bmatrix}^T
\tag{62}
$$

Then the nonlinear state-space model follows from Eqs. (1) and (2) as

$$
\dot{\mathbf{X}} = \mathbf{f}(\mathbf{X}) \equiv
\begin{bmatrix}
x_4 \\
x_5 \\
x_6 \\
x_1 x_{10}^2 \left(1 + 2x_7/p\right) + 2x_{10}\left(x_5 - x_2 x_8/x_7\right) \\
-2x_{10}\left(x_4 - x_1 x_8/x_7\right) + x_2 x_{10}^2 \left(1 - x_7/p\right) \\
-x_7 x_{10}^2 x_3/p \\
x_8 \\
x_7 x_{10}^2 \left(1 - x_7/p\right) \\
x_{10} \\
-2x_8 x_{10}/x_7
\end{bmatrix}
\tag{63}
$$

In this formulation the chief radius and true anomaly, as well as their respective derivatives, are estimated. The observability of these quantities from relative position measurements is discussed in Ref. 26. If this information is assumed known *a priori*, then these states can removed and their respective measured values can be added as process noise in the state model. The error-state vector for the chief and deputy gyro bias case is now a combination of Eqs. (41) and (62):

$$
\Delta \mathbf{x} \equiv \begin{bmatrix} \boldsymbol{\delta\alpha}^T & \Delta\boldsymbol{\beta}_c^T & \Delta\boldsymbol{\beta}_d^T & \Delta\boldsymbol{\rho}^T & \Delta\dot{\boldsymbol{\rho}}^T & \Delta r_c & \Delta\dot{r}_c & \Delta\theta & \Delta\dot{\theta} \end{bmatrix}^T
\tag{64}
$$

with obvious definitions of $\Delta\boldsymbol{\rho}$, $\dot{\boldsymbol{\rho}}$, Δr_c, $\Delta\dot{r}_c$, $\Delta\theta$ and $\Delta\dot{\theta}$. The matrices F and G that are used in the EKF covariance propagation are given by

$$
F = \begin{bmatrix}
-[\hat{\boldsymbol{\omega}}_d\times] & A(\hat{\mathbf{q}}) & -I_{3\times3} & 0_{3\times10} \\
0_{3\times3} & 0_{3\times3} & 0_{3\times3} & 0_{3\times10} \\
0_{3\times3} & 0_{3\times3} & 0_{3\times3} & 0_{3\times10} \\
0_{10\times3} & 0_{10\times3} & 0_{10\times3} & \left.\frac{\partial \mathbf{f}(\mathbf{X})}{\partial \mathbf{X}}\right|_{\hat{\mathbf{X}}}
\end{bmatrix}
\tag{65a}
$$

$$
G = \begin{bmatrix}
A(\hat{\mathbf{q}}) & -I_{3\times3} & 0_{3\times3} & 0_{3\times3} & 0_{3\times3} \\
0_{3\times3} & 0_{3\times3} & I_{3\times3} & 0_{3\times3} & 0_{3\times3} \\
0_{3\times3} & 0_{3\times3} & 0_{3\times3} & I_{3\times3} & 0_{3\times3} \\
0_{3\times3} & 0_{3\times3} & 0_{3\times3} & 0_{3\times3} & 0_{3\times3} \\
0_{3\times3} & 0_{3\times3} & 0_{3\times3} & 0_{3\times3} & I_{3\times3} \\
0_{2\times3} & 0_{2\times3} & 0_{2\times3} & 0_{2\times3} & 0_{2\times3} \\
0_{2\times3} & 0_{2\times3} & 0_{2\times3} & 0_{2\times3} & 0_{2\times3}
\end{bmatrix}
\tag{65b}
$$

where $\hat{\mathbf{X}}$ denotes the estimate of $\mathbf{X}$. The partial matrix $\partial\mathbf{f}(\mathbf{X})/\partial\mathbf{X}$ is straightforward to derive and is not shown here for brevity. Defining the new process noise vector as $\mathbf{w} \equiv \begin{bmatrix} \boldsymbol{\eta}_{cv}^T & \boldsymbol{\eta}_{dv}^T & \boldsymbol{\eta}_{cu}^T & \boldsymbol{\eta}_{du}^T & w_x & w_y & w_z \end{bmatrix}^T$, then

the new matrix Q is given by

$$Q = \begin{bmatrix} \sigma_{cv}^2 I_{3\times3} & 0_{3\times3} & 0_{3\times3} & 0_{3\times3} & 0_{3\times1} & 0_{3\times1} & 0_{3\times1} \\ 0_{3\times3} & \sigma_{dv}^2 I_{3\times3} & 0_{3\times3} & 0_{3\times3} & 0_{3\times1} & 0_{3\times1} & 0_{3\times1} \\ 0_{3\times3} & 0_{3\times3} & \sigma_{cu}^2 I_{3\times3} & 0_{3\times3} & 0_{3\times1} & 0_{3\times1} & 0_{3\times1} \\ 0_{3\times3} & 0_{3\times3} & 0_{3\times3} & \sigma_{du}^2 I_{3\times3} & 0_{3\times1} & 0_{3\times1} & 0_{3\times1} \\ 0_{1\times3} & 0_{1\times3} & 0_{1\times3} & 0_{1\times3} & w_x & 0 & 0 \\ 0_{1\times3} & 0_{1\times3} & 0_{1\times3} & 0_{1\times3} & 0 & w_y & 0 \\ 0_{1\times3} & 0_{1\times3} & 0_{1\times3} & 0_{1\times3} & 0 & 0 & w_z \end{bmatrix} \tag{66}$$

The sensitivity matrix is also modified to be

$$H_k(\hat{\mathbf{q}}_k^-, \hat{\boldsymbol{\rho}}_k^-) = \begin{bmatrix} [A(\hat{\mathbf{q}}^-)\hat{\mathbf{r}}_1^- \times] & 0_{3\times3} & 0_{3\times3} & \dfrac{\partial \hat{\mathbf{b}}_1^-}{\partial \hat{\boldsymbol{\rho}}^-} & 0_{3\times7} \\ \vdots & \vdots & \vdots & \vdots & \vdots \\ [A(\hat{\mathbf{q}}^-)\hat{\mathbf{r}}_N^- \times] & 0_{3\times3} & 0_{3\times3} & \dfrac{\partial \hat{\mathbf{b}}_N^-}{\partial \hat{\boldsymbol{\rho}}^-} & 0_{3\times7} \end{bmatrix}_{t_k} \tag{67}$$

where $\hat{\mathbf{r}}_i^-$ is given by Eq. (6b) evaluated at $\hat{\boldsymbol{\rho}}^- \equiv [\hat{x}^- \quad \hat{y}^- \quad \hat{z}^-]^T$ and the partial matrix $\partial \hat{\mathbf{b}}_i^- / \partial \hat{\boldsymbol{\rho}}^-$ is given by

$$\frac{\partial \hat{\mathbf{b}}_i^-}{\partial \hat{\boldsymbol{\rho}}^-} = A(\hat{\mathbf{q}}^-) \frac{\partial \hat{\mathbf{r}}_i^-}{\partial \hat{\boldsymbol{\rho}}^-} \tag{68}$$

where

$$\frac{\partial \hat{\mathbf{r}}_i^-}{\partial \hat{\boldsymbol{\rho}}^-} = \frac{1}{\hat{s}_i^-} \begin{bmatrix} -\left[(Y_i - \hat{y}^-)^2 + (Z_i - \hat{z}^-)^2\right] & (X_i - \hat{x}^-)(Y_i - \hat{y}^-) & (X_i - \hat{x}^-)(Z_i - \hat{z}^-) \\ (X_i - \hat{x}^-)(Y_i - \hat{y}^-) & -\left[(X_i - \hat{x}^-)^2 + (Z_i - \hat{z}^-)^2\right] & (Y_i - \hat{y}^-)(Z_i - \hat{z}^-) \\ (X_i - \hat{x}^-)(Z_i - \hat{z}^-) & (Y_i - \hat{y}^-)(Z_i - \hat{z}^-) & -\left[(X_i - \hat{x}^-)^2 + (Y_i - \hat{y}^-)^2\right] \end{bmatrix} \tag{69}$$

with $\hat{s}_i^- \equiv \left[(X_i - \hat{x}^-)^2 + (Y_i - \hat{y}^-)^2 + (Z_i - \hat{z}^-)^2\right]^{3/2}$. The EKF can now be executed with these new quantities to estimate both relative attitude and position.

VI. Simulation Results

In this section simulation results are presented that show the performance of the EKF to estimate both relative attitude and position between spacecraft using LOS vectors from the VISNAV sensor. For the chief spacecraft, parameters from the Hubble Space Telescope are selected. The semimajor axis is given by 6,998,455 meters and the eccentricity is $e = 0.00172$. A bounded relative orbit is used. The constraint required on the Cartesian initial conditions must then satisfy[12]

$$\frac{\dot{y}(t_0)}{x(t_0)} = \frac{-n(2+e)}{\sqrt{(1+e)(1-e)^3}} \tag{70}$$

This bounded relative orbit constraint is valid for both eccentric and circular chief orbits. Note that its form requires that t_0 be defined to be at the orbit perigee point. This is only used for simulation purposes though. The EKF can be initiated at any part of the orbit. The initial chief orbit radius and true anomaly rate are given by $r_c(t_0) = a(1 - e)$ and $\dot{\theta}(t_0) = \sqrt{\mu/p}\,(1 + e)/r_c$, where $\mu = 3.986008 \times 10^{14}$ m^3/s^2. At perigee we have $\dot{r}_c(t_0) = 0$ and $\theta(t_0) = 0$. The initial condition for the vector X in appropriate units of meters and meters per second is given by
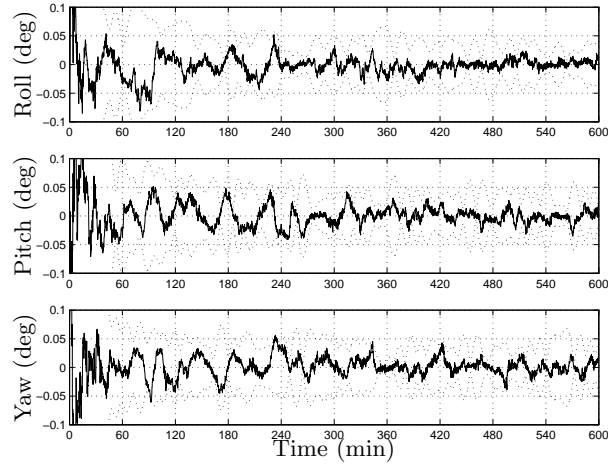
$$\mathbf{X}(t_0) = \begin{bmatrix} 200 & 200 & 100 & 0.01 & -0.4325 & 0.01 & r_c(t_0) & 0 & 0 & \dot{\theta}(t_0) \end{bmatrix}^T \tag{71}$$

The simulation time for relative motion between the two spacecraft is 600 minutes and time interval is 10 seconds. The spectral densities of the process noise components w_x, w_y and w_z in Eq. (1) are each given by
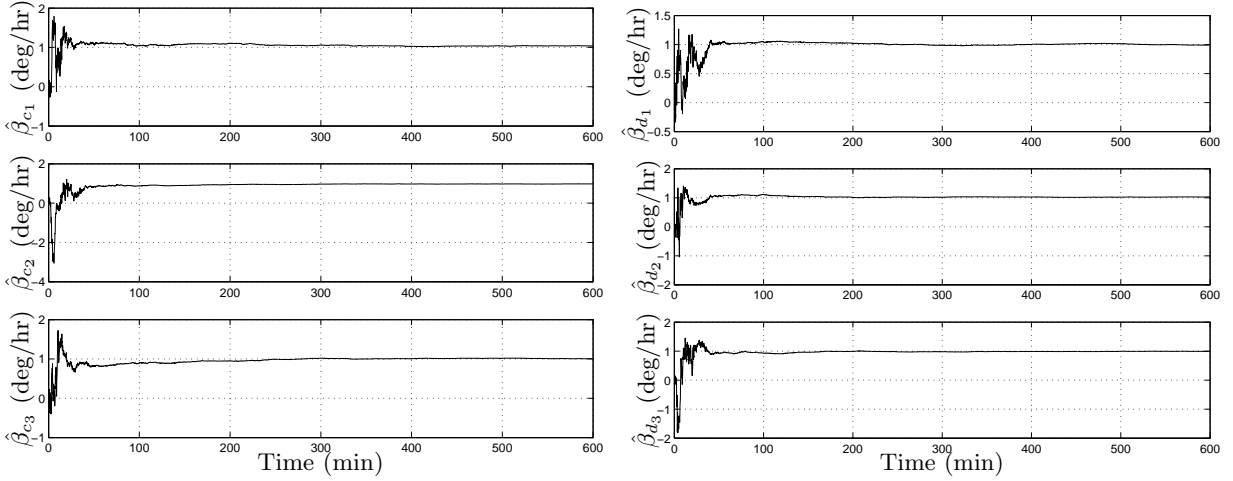
(a) Chief Bias Estimates

(b) Deputy Bias Estimates

(c) Attitude Errors and 3σ Bounds

Figure 3. Gyro Bias Estimates and Attitude Errors

$\sqrt{10} \times 10^{-11}$ m/(s$\sqrt{\text{s}}$). The orbit period of deputy is calculated to be 5,820 seconds. This period makes the deputy move about 6 times around the chief during the simulation run.

The true relative attitude motion is given by propagating Eq. (27) using an initial quaternion given by $\mathbf{q}(t_0) = [\sqrt{2}/2 \ 0 \ 0 \ \sqrt{2}/2]^T$ and angular velocities given by $\boldsymbol{\omega}_c = [0 \ 0.0011 \ -0.0011]^T$ rad/sec and $\boldsymbol{\omega}_d = [-0.002 \ 0 \ 0.0011]^T$ rad/sec for the entire simulation run. The gyro noise parameters are given by $\sigma_{cu} = \sigma_{du} = \sqrt{10} \times 10^{-10}$ rad/sec$^{3/2}$ and $\sigma_{cv} = \sigma_{dv} = \sqrt{10} \times 10^{-5}$ rad/sec$^{1/2}$. The initial biases for each axis of both the chief and deputy gyros is given by 1 deg/hr. Six beacons are assumed to exist on the chief:

$$X_1 = 0.5\text{m}, \quad Y_1 = 0.5\text{m}, \quad Z_1 = 0.0\text{m} \tag{72a}$$

$$X_2 = -0.5\text{m}, \quad Y_2 = -0.5\text{m}, \quad Z_2 = 0.0\text{m} \tag{72b}$$

$$X_3 = -0.5\text{m}, \quad Y_3 = 0.5, \quad Z_3 = 0.0\text{m} \tag{72c}$$

$$X_4 = 0.5\text{m}, \quad Y_4 = -0.5\text{m}, \quad Z_4 = 0.0\text{m} \tag{72d}$$

$$X_5 = 0.2\text{m}, \quad Y_5 = 0.5\text{m}, \quad Z_5 = 0.1\text{m} \tag{72e}$$

$$X_6 = 0.0\text{m}, \quad Y_6 = 0.2\text{m}, \quad Z_6 = -0.1\text{m} \tag{72f}$$

(a) True and Estimated Position Comparison

(b) Position Errors and 3σ Bounds

(c) Velocity Errors and 3σ Bounds

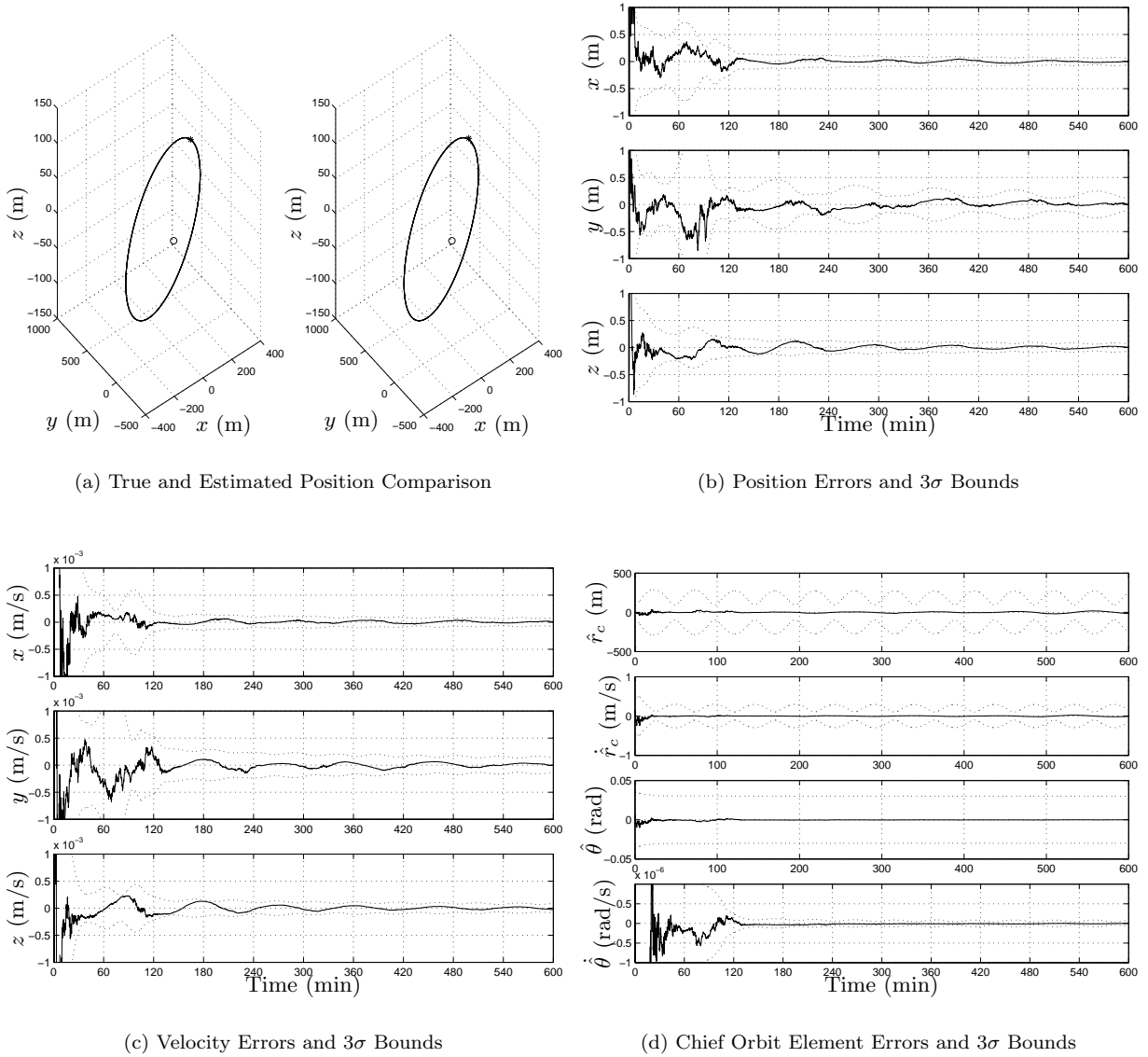(d) Chief Orbit Element Errors and 3σ Bounds

Figure 4. Orbit Element Estimates

These beacons are assumed to be visible to the PSD on the deputy throughout the entire simulation run. Simulated VISNAV measurements are generated using Eq. (7) with a measurement standard deviation given by 0.0005 degrees.

In order to initialize the EKF a nonlinear least squares routine from the synthetic measurements is used to determine the initial relative attitude and position. Each individual covariance sub-matrix for attitude, gyro biases, position and velocity is assumed to be isotropic, i.e. a diagonal matrix with equal elements. The initial attitude covariance is given by $I_{3\times3}$ deg^2. The initial chief and deputy gyro bias covariances are each set to $4I_{3\times3}$ (deg/hr)^2. The initial position covariance is set to $5I_{3\times3}$ m^2 and the initial velocity covariance is set to $0.02I_{3\times3}$ (m/s)^2. The initial variance for the chief position is set to 1,000 m^2 and the velocity variance is set to 0.01 (m/s)^2. The initial variance for the true anomaly is set to 1×10^{-4} rad^2 and the rate variance is set to 1×10^{-4} (rad/sec)^2.

Figures 3(a) and 3(b) show the chief and deputy bias estimates, which are all well estimated by the EKF. Figure 3(c) shows the attitude errors and respective 3σ bounds derived from the EKF covariance matrix. All errors remain within their respective bounds, which indicates that the EKF is working properly. The attitude errors are within 0.05 degrees. Figure 4(a) shows a comparison between the true and estimated

position, with the errors shown in Figure 4(b). Relative position knowledge is within 0.3 meters for each axis. Figure 4(c) shows the relative velocity errors, which shows that velocity knowledge is within 2×10^{-4} meters per second. The chief orbital element errors are shown in Figure 4(d). The chief radius has a maximum 3σ bound of about 300 meters, although the actual errors are much smaller. The velocity errors are well below 1 meter per second. The true anomaly 3σ bound shows that its estimate error may be fairly large, up to about 2 degrees, although the actual errors are much smaller. The true anomaly rate is known to within 1×10^{-7} rad/sec. The accuracy of these estimates not only depends on the accuracy of the PSD sensor and the number of beacons, but also on the "spread" of the beacons as well as the distance from the beacons and PSD. From Figures 3(c) and 4(b) the attitude and position covariance increases just past 60 minutes, which intuitively makes sense since this coincides with the maximum relative distance between the spacecraft. Still, the simulation results indicate that using a filter with gyros and an orbital dynamic model significantly increases the accuracy over a deterministic solution by at least 2 orders of magnitude.

VII. Conclusions

An extended Kalman filter has been designed for relative navigation and attitude determination of space-craft. The measurements were assumed to be given by line-of-sight observations using a novel sensing approach involving beacons and position sensing technology in the focal plane. For attitude estimation three different filter formulations were presented. The first directly estimated the chief and deputy gyro biases. The second estimated the relative rate and deputy gyro biases, and the third estimated the relative rate and chief gyro biases. For position estimation a nonlinear orbital model was used, where perturbation were modelled by process noise. Simulation results have shown that the combined relative attitude/position Kalman filter is able to achieve accurate results using a close configuration of beacons with a modest relative distance between spacecraft. It is important to note that the filter developed in this paper estimates not only the deputy states, but also the chief states including the chief radius, true anomaly and gyro biases. In actual practice, the chief parameters will be known through external sensors onboard the chief spacecraft. For this more practical case, the states in the filter design presented here can be reduced to only deputy associated parameters. Still, this paper has shown that it is also possible to estimate both chief and deputy states if desired.

References

[1] Robertson, A., Corazzini, T., LeMaster, F., and How, J. P., "Formation Sensing and Control Technologies for a Separated Spacecraft Interferometer," *Proceedings of the 1998 American Control Conference*, Philadelphia, PA, June 1998, pp. 1574–1580.

[2] Carpenter, J., Leitner, J., Folta, D., and Burns, R., "Benchmark Problems for Spacecraft Formation Flying Missions," *AIAA Guidance, Navigation, and Control Conference*, Austin, TX, Aug. 2003, AIAA 2003-5364.

[3] Corazzini, T., Robertson, A., Adams, J. C., Hassibi, A., and How, J. P., "GPS Sensing for Spacecraft Formation Flying," *ION-GPS-97 Conference*, Kansas, MO, Sept. 1997.

[4] Purcell, G., Kuang, D., Lichten, S., Wu, S. C., and Young, L., "Autonomous Formation Flyer (AFF) Sensor Technology Development," *AAS Guidance and Control Conference*, Breckenridge, CO, Feb. 1998, AAS 98-062.

[5] Alonso, R., Crassidis, J. L., and Junkins, J. L., "Vision-Based Navigation for Formation Flying of Spacecraft," *AIAA Guidance, Navigation, and Control Conference*, Denver, CO, August 2000, AIAA 2000-4439.

[6] Junkins, J. L., Hughes, D. C., Wazni, K. P., and Pariyapong, V., "Vision-Based Navigation for Rendezvous, Docking and Proximity Operations," *22nd Annual AAS Guidance and Control Conference*, Breckenridge, CO, Feb. 1999, AAS 99-021.

[7] Hill, G., "Researches in the Lunar Theory," *American Journal of Mathematics*, , No. 1, 1878, pp. 5–26.

[8] Clohessy, W. and Wiltshire, R., "Terminal Guidance System for Satellite Rendezvous," *Journal of Guidance, Control, and Dynamics*, Vol. 8, No. 2, March-April 1985, pp. 235–242.

[9] Inalhan, G., Tillerson, M., and How, J. P., "Relative Dynamics and Control of Spacecraft Formations in Eccentric Orbits," *Journal of Guidance, Control, and Dynamics*, Vol. 25, No. 1, Jan.-Feb. 2002, pp. 48–59.

[10] Alfriend, K. T., Yan, H., and Vadali, S. R., "Nonlinear Considerations in Satellite Formation Flying," *AIAA/AAS Astrodynamics Specialist Conference*, Monterey, CA, Aug. 2002, AIAA 2002-4741.

[11] Karlgaard, C. D. and Lutze, F. H., "Second-Order Relative Motion Equations," *AAS/AIAA Astrodynamics Specialist Conference*, Quebec City, Canada, July 2001, AAS 01-464.

[12] Schaub, H. and Junkins, J. L., *Analytical Mechanics of Aerospace Systems*, chap. 14, American Institute of Aeronautics and Astronautics, Inc., New York, NY, 2003.

[13] Ju, G., Pollack, T., and Junkins, J. L., "DIGISTAR II Micro-Star Tracker: Autonomous On-Orbit Calibration and Attitude Estimation," *AAS/AIAA Astrodynamics Specialist Conference*, Girdwood, Alaska, August 1999, AAS 99-431.

[14] Light, D. L., "Satellite Photogrammetry," *Manual of Photogrammetry*, edited by C. C. Slama, chap. 17, American Society of Photogrammetry, Falls Church, VA, 4th ed., 1980.

[15]Shuster, M. D. and Oh, S. D., "Three-Axis Attitude Determination from Vector Observations," *Journal of Guidance and Control*, Vol. 4, No. 1, Jan.-Feb. 1981, pp. 70–77.

[16]Cheng, Y., Crassidis, J. L., and Markley, F. L., "Attitude Estimation for Large Field-of-View Sensors," *AAS Malcolm D. Shuster Astronautics Symposium*, Grand Island, NY, June 2005, AAS-05-462.

[17]Shuster, M. D., "Kalman Filtering of Spacecraft Attitude and the QUEST Model," *The Journal of the Astronautical Sciences*, Vol. 38, No. 3, July-Sept. 1990, pp. 377–393.

[18]Farrenkopf, R. L., "Analytic Steady-State Accuracy Solutions for Two Common Spacecraft Attitude Estimators," *Journal of Guidance and Control*, Vol. 1, No. 4, July-Aug. 1978, pp. 282–284.

[19]Shuster, M. D., "A Survey of Attitude Representations," *Journal of the Astronautical Sciences*, Vol. 41, No. 4, Oct.-Dec. 1993, pp. 439–517.

[20]Lefferts, E. J., Markley, F. L., and Shuster, M. D., "Kalman Filtering for Spacecraft Attitude Estimation," *Journal of Guidance, Control, and Dynamics*, Vol. 5, No. 5, Sept.-Oct. 1982, pp. 417–429.

[21]Xing, G. Q. and Parvez, S. A., "Nonlinear Attitude State Tracking Control for Spacecraft," *Journal of Guidance, Control, and Dynamics*, Vol. 24, No. 3, May-June 2001, pp. 624–626.

[22]Markley, F. L., "Matrix and Vector Algebra," *Spacecraft Attitude Determination and Control*, edited by J. R. Wertz, appendix C, Kluwer Academic Publishers, The Netherlands, 1978, p. 755.

[23]Crassidis, J. L. and Junkins, J. L., *Optimal Estimation of Dynamic Systems*, chap. 7, Chapman & Hall/CRC, Boca Raton, FL, 2004.

[24]van Loan, C. F., "Computing Integrals Involving the Matrix Exponential," *IEEE Transactions on Automatic Control*, Vol. AC-23, No. 3, June 1978, pp. 396–404.

[25]Sun, D. and Crassidis, J. L., "Observability Analysis of Six-Degree-of-Freedom Configuration Determination Using Vector Observations," *Journal of Guidance, Control, and Dynamics*, Vol. 25, No. 6, Nov.-Dec. 2002, pp. 1149–1157.

[26]Psiaki, M. L., "Autonomous Orbit Determination for Two Spacecraft from Relative Position Measurements," *Journal of Guidance, Control, and Dynamics*, Vol. 22, No. 2, March-April 1999, pp. 305–312.